Monte Carlo simulation of submonolayer vapor-deposition polymerization

Y.-P. Zhao,[1] A. R. Hopper,[2] G.-C. Wang,[1] and T.-M. Lu[1]
[1]*Department of Physics, Applied Physics, and Astronomy, Rensselaer Polytechnic Institute, Troy, New York 12180-3590*
[2]*College of Engineering and Physical Sciences, University of New Hampshire, Durham, New Hampshire 03824*
(Received 16 November 1998; revised manuscript received 16 June 1999)

In this paper, we propose a Monte Carlo simulation model for the initial growth of polymer films by considering only monomer surface diffusion in the vapor-deposition polymerization process. In the model, monomers are deposited randomly on a two-dimensional square lattice with periodic boundary conditions and are allowed to diffuse with nearest neighbor hops. Whenever monomers meet, they stop diffusing and form a stable dimer. When a diffusing or deposited monomer encounters one of the ends of a polymer ($L>1$), it stops moving and attaches to the polymer. Attachment of monomers or other polymers is allowed only at the two ends of the polymer. We have shown that there are three distinct growth regimes for surface coverages $\theta<0.5$: a low-coverage initiation regime (*I*), a chain propagation regime (*P*), and a saturation regime (*S*). In both regimes *I* and *P*, the growth is similar to the molecular beam epitaxy model. We examine in detail the scaling relations for the chain length distribution, which agree quite well with results of a rate equation. However, in regime *S*, our model gives very different kinetics. The breakdown of scaling at higher coverages is due to the fact that long-chain polymers have partitioned the lattice with inactive sites. This inhibits further polymer growth and enhances production of dimers, shifting the chain distribution to favor shorter polymers and driving the average molecular weight down. The chain configuration initially is similar to a path taken in a diffusion-limited self-avoiding walk. However, at high coverages, due to the correlation of long polymer chains, the polymer chains tend to be compact. [S1063-651X(99)02910-4]

PACS number(s): 81.15.−z, 68.55.−a, 81.10.Bk

I. INTRODUCTION

Recently there has been great technological interest in polymer thin films as candidates for a low-*k* dielectric interlayer for microelectronic interconnects [1]. The most widely used coating method for polymer thin films is the spin-on technique. Another very attractive method for future semiconductor products is vapor deposition [1], which has the advantage that it is a dry process. Vapor deposition provides an extremely uniform coating over a very large area, and it possesses superior gap-filling capability. One of the most well studied vapor-deposited polymers is Xylylene [1,2]. The coating process is best described as vapor-deposition polymerization (VDP), in which monomers from the gas phase condense on the substrate and react to form high molecular weight, linear poly(*p*-xylylene) (PPX), or Parylene. For example, Fig. 1 shows the conventional process for producing Parylene-*N* (PA-*N*) films by VDP using the precursor material di-*p*-xylylene (dimer). During the VDP process, the dimer molecules are sublimed at 150 °C and then pyrolized into monomers at 650 °C. The monomers condense and polymerize on a Si wafer at room temperature. As suggested by Beach *et al.* [2,3], both the condensation and diffusion of monomers occur in a VDP process. The monomers can be consumed by two chemical reactions: initiation, in which new polymer molecules are generated, and propagation, in which existing polymer molecules are extended to higher molecular weight. Beach considered a general bulk growth model for the Parylene VDP process [3], which Ganguli *et al.* [4] later extended. However, the initial stages of the VDP process have not been well studied.

The initial stages of a VDP process are quite different from the initial polymerization process in a solution. For the polymerization process in a solution, the concentration of the monomer solution is fixed. A monomer in the solution undergoes random walks until it meets with another walker or polymer and will form a polymer or lengthen an existing polymer chain. One of the simple models for monomers in a solution is the self-avoiding walk (SAW), which was widely studied in the polymer community [5]. A SAW is a random walk with an excluded volume constraint—which is a walk that is not allowed to intersect itself. In general, the mean square end-to-end distance, $\langle R^2 \rangle$, and the length of the walk, *d*, have the relation

$$\langle R^2 \rangle \sim d^{2\nu}, \tag{1}$$

where the exponent ν is the reciprocal of the fractal dimensionality D_ν of a SAW chain. For a two-dimensional SAW, $\nu = \frac{3}{4}$ [5]. A modified model is the diffusion-limited self-avoiding walk (DLSAW), in which bifunctional monomers diffuse from far away to the growing tip of a linear polymer [6]. This model gives $\nu = 0.774 \pm 0.006$ for a two-dimensional square lattice. Meakin extended this model to describe the formation of multipolymer chains from solution and found $D_\nu = 1.23 \pm 0.03$ for two dimensions [7]. For a VDP process, the monomers are confined to a solid substrate,

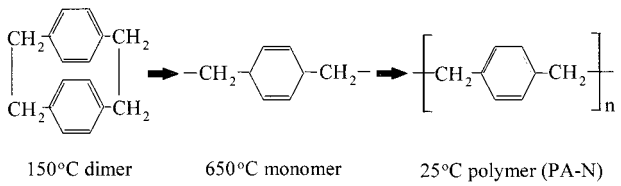

FIG. 1. Vapor-deposition polymerization process of Parylene-*N* and its chemical structures.

and they can move only along the substrate surface. The process would be similar to the two-dimensional DLSAW except that the number of nucleation centers keeps increasing.

Monomer transport in vacuum during VDP process is very much like the conventional physical vapor-deposition (PVD) process or molecular beam epitaxy (MBE) process for metals or semiconductors, in which atoms or molecules condense from the gas phase onto the substrate. The differences between VDP and either PVD or MBE lie in the nucleation process after the monomers have condensed on the substrate. In PVD or MBE processes, atoms can nucleate at the nearest neighbors of the nucleated sites. Also there are many other atomistic processes such as surface diffusion, edge diffusion, step barrier effect, etc., that can affect the submonolayer growth. Recently scaling properties have been studied for submonolayer PVD or MBE growth through Monte Carlo simulations by considering some simple atomistic processes such as surface diffusion [8,9], island diffusion [10], and edge diffusion [11]. In the simplest model, in which only surface diffusion [8,9] was considered, it was found that, during the deposition, the cluster size and total cluster density depend largely on the ratio $G=D_s/F$, where F is the deposition rate and D_s is the surface diffusion coefficient for adatoms. For low surface coverages, there exists a dynamic scaling relationship for the cluster size distribution $N_s(t)$:

$$N_s(\theta)=\theta S^{-2}f(s/S), \tag{2}$$

where the surface coverage $\theta=Ft=\Sigma_{s\geqslant 1}sN_s$, the average cluster size $S=\Sigma_{s\geqslant 2}sN_s(\theta)/\Sigma_{s\geqslant 2}N_s(\theta)=(\theta-N_1)/N$, N_1 is the monomer density, and $N=\Sigma_{s\geqslant 2}N_s(\theta)$ is the total cluster density. The $f(x)$ is a scaling function. Both the average cluster size S and the total cluster density N scale as

$$S\propto G^{\chi}\theta^{z}, \tag{3}$$

$$N\propto G^{-\chi}\theta^{1-z}, \tag{4}$$

where the exponent χ represents the scaling of the cluster density at a fixed coverage, and the exponent z indicates the scaling of the average cluster size at a fixed ratio G. At higher coverages, the clusters coalesce and undergo a percolation transition. For the VDP process, the reaction occurs only at the ends of a polymer. The other processes could be surface diffusion, intermolecular interaction, relaxation, etc. The latter two processes are very different from the atomistic processes for PVD or MBE, and should give a distinct dynamic behavior for the VDP process.

In this paper, we propose a simple model for the initial growth of polymers by considering only monomer surface diffusion in the VDP process. We consider only surface coverages with $\theta<0.5$. We examine in detail the scaling relations of the mean square end-to-end distance, polymer size distribution (same as cluster size distribution), total molecular density (same as total cluster density), and average molecular weight (same as average cluster size) defined in Eqs. (1)–(4) above. We also compare our results with those of the submonolayer MBE process where only surface diffusion [8,9] was considered. (Whenever we mention the MBE process in the text we refer to this surface diffusion process).

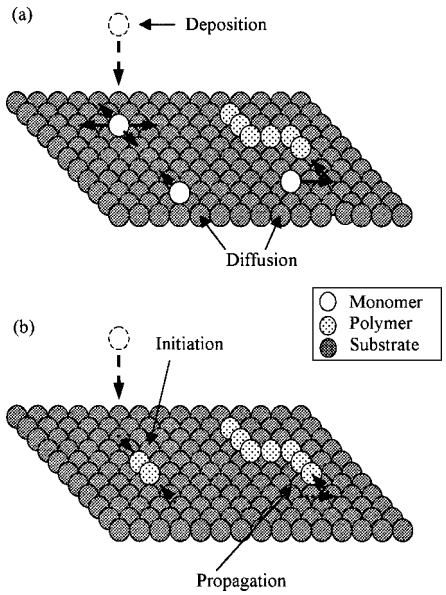

FIG. 2. Schematic representations of the basic processes considered in the VDP model, (a) monomer deposition and surface diffusion; (b) polymer initiation and propagation.

II. MODEL ASSUMPTIONS AND SIMULATION METHOD

Monomers are deposited randomly on a two-dimensional (2D) substrate and are allowed to diffuse with nearest neighbor hops as shown in Fig. 2. Whenever monomers meet they stop diffusing and form a stable dimer of chain length $L=2$. This is the so-called initiation process according to Beach [3]. When a diffusing or deposited monomer encounters the end of a polymer, it stops moving and is attached to the polymer. Also, two polymers can join together when the ends of the two polymers meet. This is the propagation process [3]. Note that, for a linear polymer, only the two ends of the chain are active, and are ready for reacting with monomers or ends of other polymers. Therefore the chain portion excluding the two ends of the polymer, or chain body, is *not* allowed to react with a monomer and cannot create another active growing site.

The simulations were performed on a 512×512 square lattice with periodic boundary conditions. The algorithm we used is straightforward: First, a monomer is randomly deposited on the substrate. Then all of the monomers on the surface move D steps randomly (where D is proportional to the surface diffusion coefficient D_s), subject to the following rules. During the deposition or random walks, if a monomer meets another monomer, a new, immobile dimer is nucleated. A monomer meeting an end of a polymer becomes incorporated into that polymer. Monomers are not allowed to move atop a polymer body, but are allowed to move away from a polymer body. No multilayer growth is allowed in the model, which means that steps to occupied sites are rejected. Also, no polymer rings are allowed to form. Only excluded volume interactions are allowed (no more than one monomer may occupy a given lattice site). A total of 100 000 monomers is deposited for each simulation onto a 512×512 square lattice (a maximum surface coverage equal to 0.381). These restrictions ensure submonolayer growth. Data are obtained from an average of ten simulations for each value of the diffusion steps D. Simulations were performed with D rang-

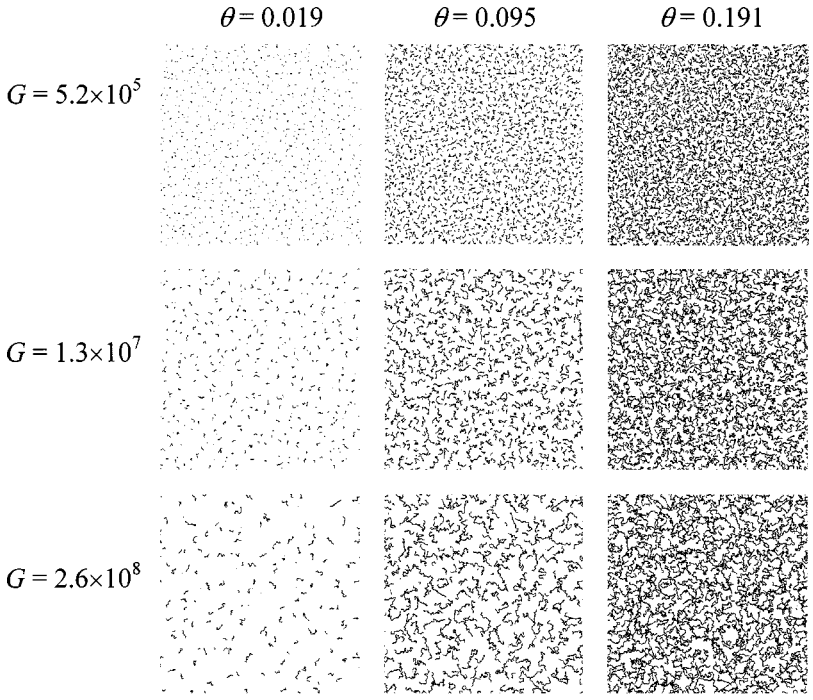

FIG. 3. Snapshots of the surface morphology for three different values of the ratio $G=5.2\times10^5$, 1.3×10^7, 2.6×10^8 and three different coverages θ=0.019, 0.095, and 0.191.

ing from 1 to 10^3 by fixing the deposition rate F at $1/512^2$ monomer per unit time per site. Therefore, $G=D\times512^2$.

The overall morphology of the polymer-covered surface was checked using a box-counting method [12], from which the fractal dimension D_f of the overall surface morphology was determined. The polymer chain configuration with a fractal dimension D_v was also investigated using Eq. (1).

III. RESULTS

A. Simulated surface morphology

Throughout the simulation, snapshots of the surface were collected. Figure 3 shows the morphology of the surface for $G=5.2\times10^5$, 1.3×10^7, and 2.6×10^8, each at coverages θ=0.019, 0.095, and 0.191. For low surface coverages, isolated wormlike linear chains formed on the surface. When the coverage increased, the chains became longer and started to join with each other. This means that at least one site in a chain was the nearest neighbor of a site in another chain. However, these chains do not really react with each other, i.e., they are still two separated polymer chains. At higher coverages, the surface formed a network structure, and the joined chains divided the surface into many empty subareas. One can imagine that one monomer deposited into one of these subareas has less of a chance to escape and has a greater tendency to initiate new polymers when another monomer comes into the area. Variations in the evolution of surface morphology were also apparent for different values of the ratio G. In particular, it is interesting to note that surfaces grown with a higher ratio G seemed to have larger areas partitioned by longer polymers, which is consistent with the results of the MBE submonolayer growth model [8,9].

B. Three distinct growth regimes

There were three distinct growth regimes for surface coverage $\theta<0.5$: a low-coverage initiation regime (I), a chain propagation regime (P), and a saturation regime (S). Figure 4 shows plots of the average molecular weight W and the total polymer density N as a function of coverage for various values of the ratio G. Here, W has the same definition as the average cluster size, and N has the same meaning as the cluster density as defined by Eqs. (3) and (4) (note that all the densities we mention below are defined as cluster number per site). The three growth regimes, separated by dotted lines, are labeled I, P, and S, respectively. Figure 5 plots the monomer density N_1 as a function of the coverage θ in log-log scale. The initiation regime was a transient regime at very low coverage for which W, N, and N_1 increase with θ. This regime has been well studied in MBE growth [9]. The behavior in this regime was not very different from that of MBE growth. In the propagation regime, W increased with θ and peaked at a certain coverage θ_p. The peak coverage θ_p decreased with increasing G. The polymer density N increased, and the monomer density N_1 increased monotonically with θ. For $\theta>\theta_p$, W decreased while N increased dramatically, which means that many short-chain polymers were formed in this regime. However, N_1 still increased monotonically; in fact, it increased linearly with the coverage. The behaviors in the latter two regimes (P and S) were quite different from those in MBE growth.

C. Scaling behaviors in the propagation and saturation regimes

Next we concentrate on the propagation regime and the saturation regime. The solid curves in the propagation regime of Fig. 4 are the best fits using Eqs. (5) and (6),

$$W\propto G^{\chi}\theta^{z}, \tag{5}$$

$$N\propto G^{-\chi}\theta^{\varepsilon}. \tag{6}$$

The fits of W and N as a function of θ gave almost constant z and ε for different ratios G: $z=0.69\pm0.02$ and $\varepsilon=0.31$

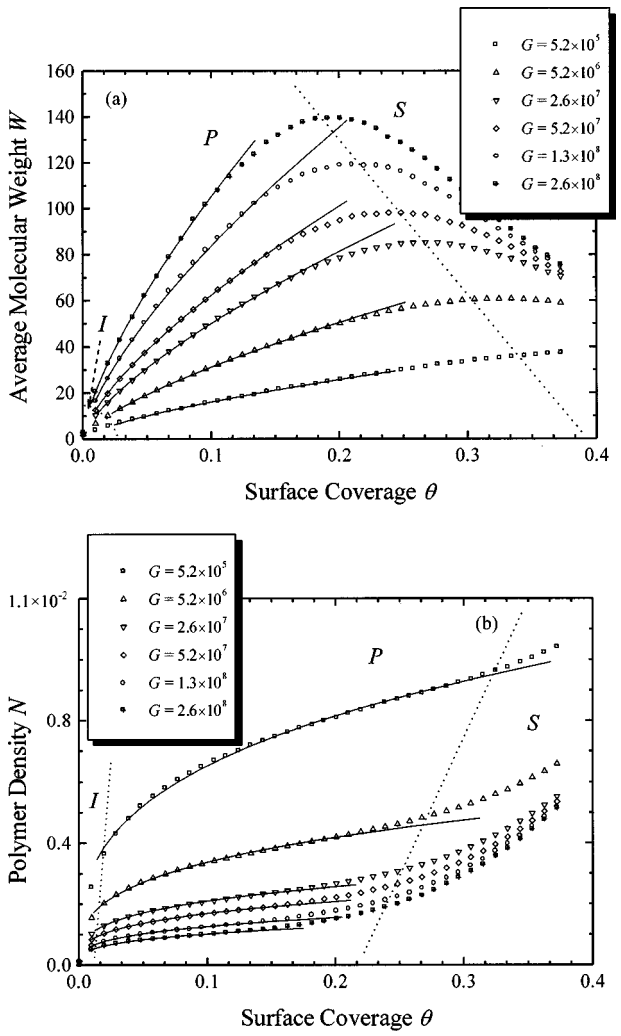

FIG. 4. (a) Average molecular weight W and (b) polymer density N plotted as a function of coverage θ for various values of G. The dashed lines divide the plots into three regimes: initiation (I), propagation (P), and saturation (S). The solid curves in the propagation regime in both plots are the best fits according to scaling relations Eqs. (5) and (6), which give $z=0.69\pm0.02$, and $\varepsilon=0.31\pm0.02$.

±0.02. The relation $\varepsilon=1-z$ held very well when describing the behavior of $W(\theta)$ and $N(\theta)$ for $\theta<\theta_p$.

We also investigate the effect of G values on W and N. Figure 6 plots the average molecular weight W and polymer density N as a function of G at various surface coverages θ. From both plots, we obtained the same exponent $\chi(\chi=0.302\pm0.002)$ for $\theta<0.2$. The agreement between $W(G)$ and $N(G)$ held for coverages $\theta<0.2$. It is interesting to note that the value obtained for χ was similar to that obtained by Amar, Family, and Lam ($\chi=0.34$) from a kinetic Monte Carlo simulation of a MBE process with a critical cluster size $i=1$ (corresponding to a stable cluster configuration of a dimer) [9], although our method is not a standard kinetic Monte Carlo simulation. The simulations of VDP and MBE (for $i=1$) were equivalent up to the formation of dimers, after which there is a divergence in the VDP model due to restrictions imposed on monomer-polymer and polymer-polymer interactions. The similarities in the physical processes of VDP and MBE have been discussed above. For θ

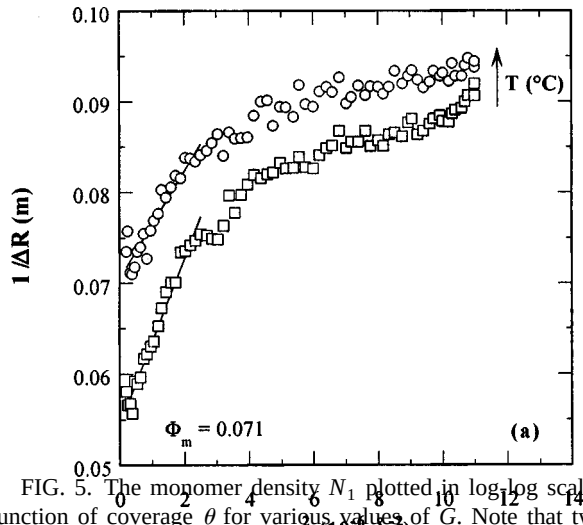

FIG. 5. The monomer density N_1 plotted in log-log scale as a function of coverage θ for various values of G. Note that two regimes separated by different slopes at different coverages (depending on the G value) can be observed clearly. The monomer density keeps on growing, which is quite different from the MBE growth model.

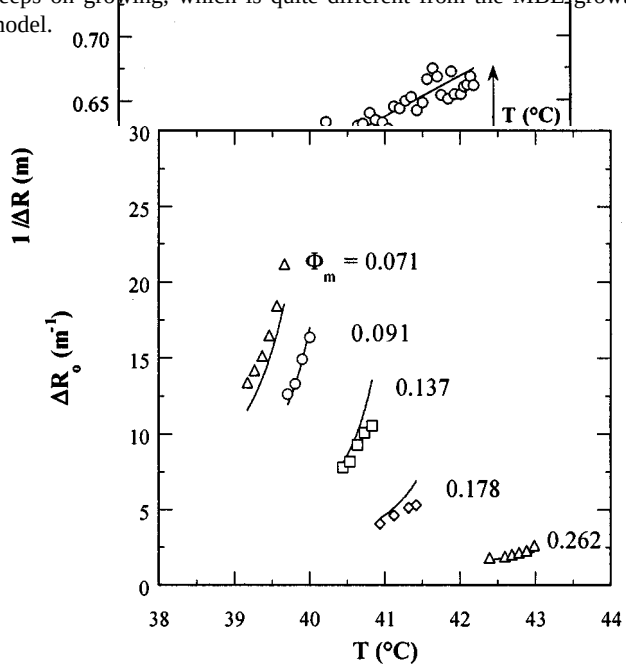

FIG. 6. (a) Average molecular weight W and (b) polymer density N plotted as a function of G for various values of θ in log-log scale. The open symbols with dashed curves represent the propagation regime. The filled symbols and solid curves represent the saturation regime. Note that even for higher coverages, for small G values, all the curves including both high and low coverages are parallel to each other with a similar slope.

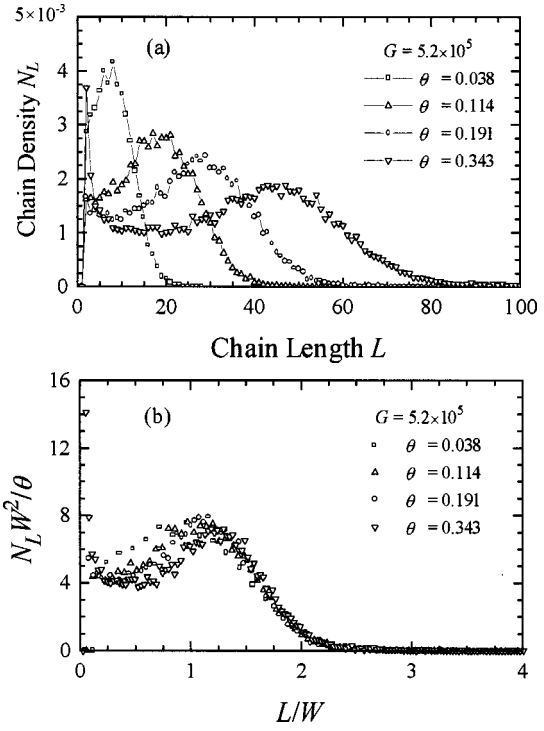

FIG. 7. (a) Unscaled polymer chain length distribution $N_L(\theta)$ and (b) scaled chain length distribution for $G=5.2\times10^5$ and θ=0.038, 0.114, 0.191, and 0.343.

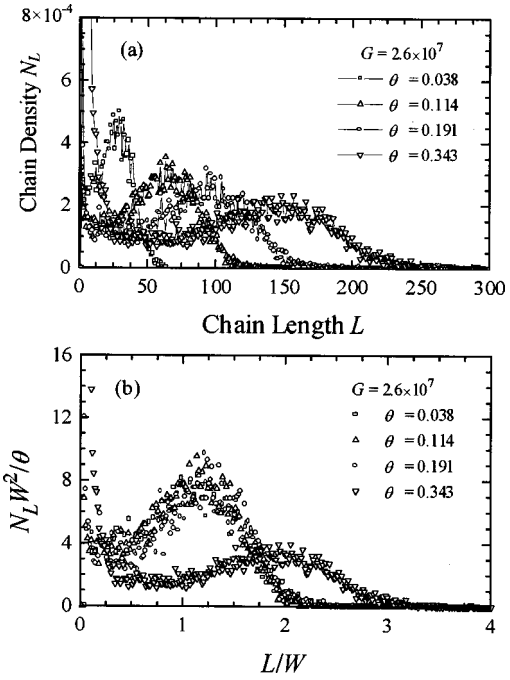

FIG. 8. (a) Unscaled polymer chain length distribution $N_L(\theta)$ and (b) scaled chain length distribution for $G=2.6\times10^7$ and θ=0.038, 0.114, 0.191, and 0.343. Note that the scaling breaks down for $\theta>0.2$.

>0.2, as shown in Fig. 6, the scaling broke down for large G values. However, for small G values, the scaling relation can be extended to higher θ, because θ_p for small G values is larger than θ_p for large G values.

One very important feature in the propagation regime is the scaling of the polymer chain distributions. Figures 7 and 8 show the polymer chain distributions $N_L(\theta)$ and rescaled distributions for $G=5.2\times10^5$ and $G=2.6\times10^7$ for four values of coverage θ. For $G=5.2\times10^5$, there was only one peak in the distribution, and the rescaled distribution $N_L W^2/\theta$ scaled very well according to Eq. (2) [Fig. 7(b)]. For $G=2.6\times10^7$, there were two peaks in each distribution shown in Fig. 8(a): one at short-chain lengths and one in which the peak position in L increased, and the height (N_L) decreased, as θ increased. The height at short-chain lengths increased with increasing θ. Figure 8(b) shows the data rescaled according to the scaling relation, Eq. (2). One can see that the scaling breaks down in this model for $\theta>\theta_p$. We also notice that, with a higher G, the breakdown of the scaling occurred at a smaller coverage θ, which is consistent with that observed in Figs. 4 and 6.

As mentioned in the above discussion, the scaling relationship broke down for $\theta>\theta_p$. The different behavior for $\theta>\theta_p$ is due to the fact that long-chain polymers have partitioned the lattice with inactive sites thus inhibiting further polymer growth and enhancing the production of dimers. Therefore, the number and distribution of longer-chain polymers does not change too much while the excess of shorter polymers drives the average molecular weight down. Figure 9 shows the long-chain distributions (a) and short-chain distributions (b) for $\theta>\theta_p$ and $G=2.6\times10^7$. Note that the long-chain distributions shown in Fig. 9(a) have almost no change with increasing coverage, while the peak height of the short-chain distribution shown in Fig. 9(b) increases dramatically with increasing coverage.

D. Percolation transition in the VDP growth model

In order to further understand the above result, in Fig. 10 we plot the density of aggregate polymer clusters N_S and its derivative $dN_s/d\theta$ as a function of coverage θ for various values of G. An aggregate polymer cluster consists of a polymer and all the polymers that it is in contact with, plus all of the polymers that are in contact with these polymers, and so on. The aggregate polymer clusters reflect the contacting polymers and the overall morphology of the surface. Initially, N_S increased as a function of coverage. After N_S peaked, N_S decreased. This behavior is similar to that of the cluster density in the MBE model [9]. Note that, at high coverages, N_S decreased with different rates. There was a turning coverage θ_t at which the decreasing rate became a minimum. In Fig. 11(a) we plot the density of aggregate polymer clusters, N_S, along with chain density N_L for several small values of L (=2, 3, and 4) as a function of surface coverage for $G=5.2\times10^6$. A plot of the first derivative of N_L with respect to θ is presented in Fig. 11(b). Initially, N_S increased while N_L decreased. After N_S peaked, N_S decreased and N_L increased dramatically. The number of shorter polymers began to increase after the number of aggregate polymer clusters reached a maximum. At $\theta=\theta_t$, shown as the vertical dashed line in Fig. 11, N_L and the rate of N_L increase dramatically. This is in accord with the argument given above for partitioning in the mixed propagation and initiation regime. In order to see this more clearly, we plot both θ_p and θ_t as a function of G in Fig. 12. Both θ_p and θ_t had power law relations with G, with the powers 0.13 and

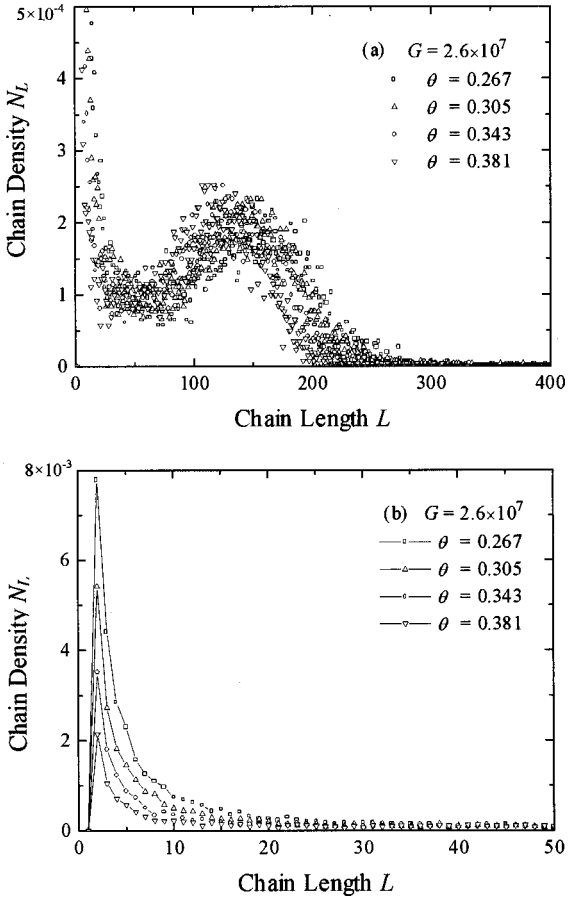

FIG. 9. (a) The long-chain distribution and (b) the short-chain distribution for $\theta > \theta_p$ and $G = 2.6\times10^7$. Note that for different coverages, the peak position and height of the long-chain distribution stay about the same, while the peak height of the short chain keeps on increasing.

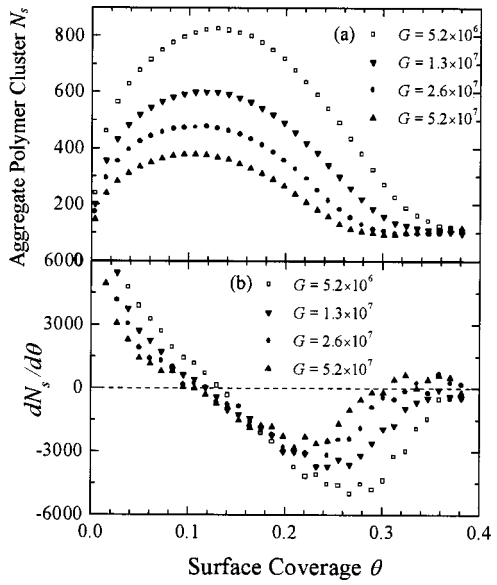

FIG. 10. (a) The density of aggregate polymer clusters, N_S, as a function of coverage θ for various values of G and (b) their derivatives with respect to coverage. The turning coverage θ_t decreases as G increases.

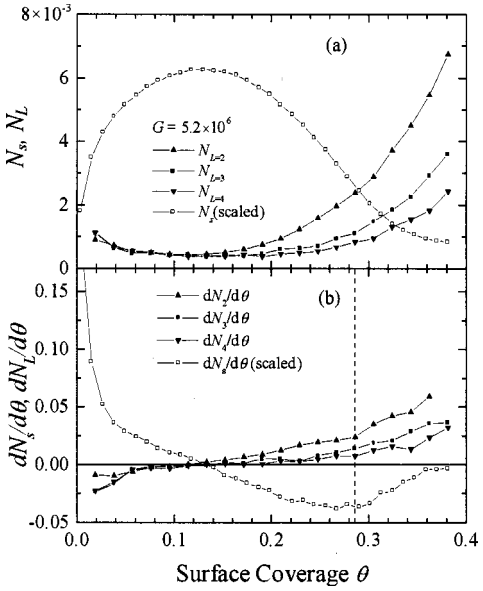

FIG. 11. (a) The density of aggregate polymer clusters N_S along with N_L for several small values of L (= 2, 3, and 4) as a function of surface coverage for $G = 5.2\times10^6$. (b) A plot of the first derivatives of N_s and N_L with respect to θ.

0.10, respectively. Considering the errors in determining θ_p and θ_t, the values of the powers are close to each other.

Figure 13 shows a plot of the largest aggregate polymer cluster versus coverage for four different values of G. The decrease of the percolation threshold coverage (the coverage at which we see a dramatic increase in the size of the largest cluster) with the ratio G is supported by the fact that, for larger values of G, longer chains are created (longer chains are able to make contacts with more sites than the shorter chains). These data support the fact that the coverage at which the scaling deviates from the power law decreases for increasing G.

E. Polymer chain configuration

Finally, we investigate the properties of the polymer chain. Figure 14 shows the relation of the mean square end-to-end distance of the polymer, $\langle R^2 \rangle$, as a function of L, and

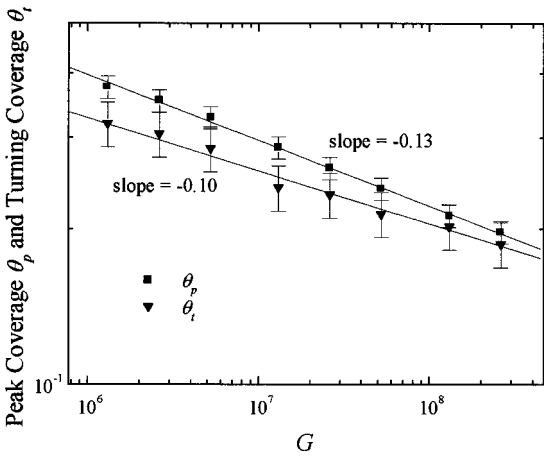

FIG. 12. The log-log plot of peak coverage θ_p and turning coverage θ_t as a function of G.

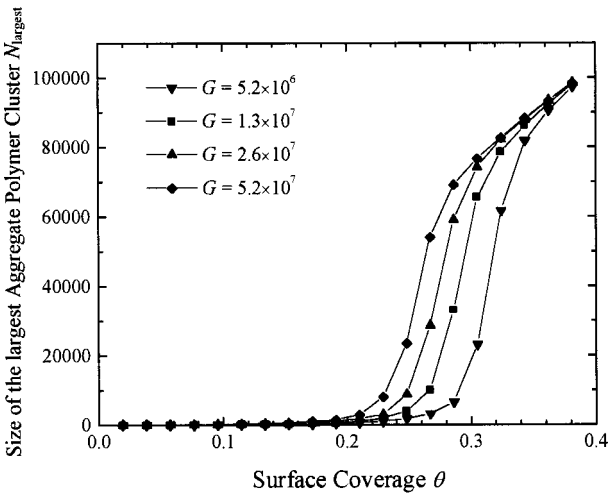

FIG. 13. The largest aggregate polymer cluster versus coverage for four different values of G: $G=5.2\times10^6$, 1.3×10^7, 2.6×10^7, and 5.2×10^7.

the values for v and D_v obtained at different coverages at a fixed $G=1.3\times10^7$. Values for the fractal dimensionality D_f obtained by box counting for a short length scale are also given (note that for a large length scale the fractal dimension obtained from the box-counting method is 2). Note that for low coverages, D_v and D_f were almost the same, but at higher coverages ($\theta>0.2$), D_v is greater than D_f. Due to the partitioning in the saturation regime, the value of v is expected to drop when $\langle R^2\rangle$ drops, which causes D_v to increase. Thus, as our chains got longer, we did not obtain a converging value of D_v. The D_f became less accurate as the surface coverage increased due to a progressive limitation in the size of the counting boxes resulting in fewer data points. We also plot in Fig. 15 the exponent v versus surface coverage θ for $G=5.2\times10^6$, 2.6×10^7, and 1.3×10^8. We note

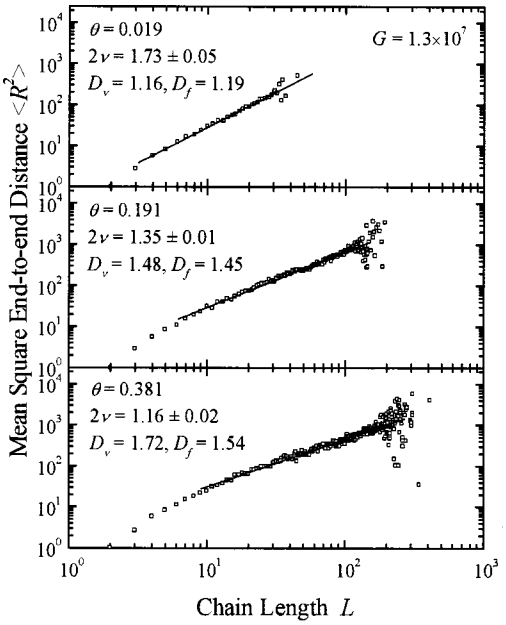

FIG. 14. The mean squared end-to-end distance of the polymer $\langle R^2\rangle$ versus chain length L for three coverages θ=0.019, 0.191, and 0.381. The slope gives the value of $2v$.

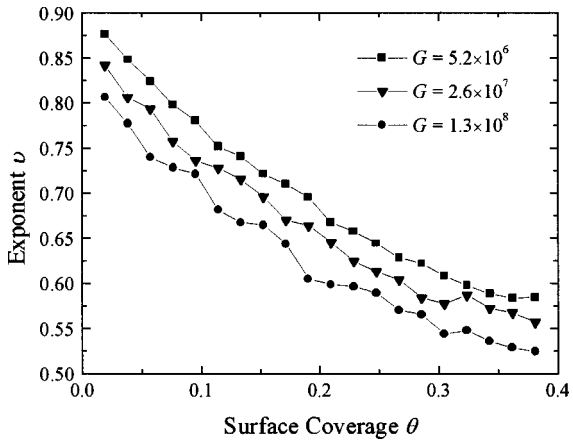

FIG. 15. The exponent v obtained from squared end-to-end distance versus surface coverage θ for $G=5.2\times10^6$, 2.6×10^7, and 1.3×10^8. Note that for a fixed coverage, when G increases, v decreases, which means large G results in more compact polymer chains.

that, for a given coverage, when G increased, v decreased, which means that a large G gives more compact chains. Also, for a given G, as θ increased, v decreased because the polymer chains became longer and more compact.

IV. DISCUSSION AND CONCLUSION

A. Comparison of the VDP growth model with the MBE growth model

In the early stage of MBE growth models [8–11], nucleation takes place easily and the cluster density increases rapidly. This essentially occurs in our VDP model because the main product of a nucleation or initiation is a dimer. However, for a MBE system, when the number of clusters increases, newly deposited atoms are more likely to join existing clusters than to meet another atom and initiate new clusters. Therefore the main effect of deposition at this stage is to increase the size of an existing cluster, and the cluster density remains constant. However, in the VDP process, because only two ends of a polymer can react with a monomer, a monomer has almost the same probability of reacting with a polymer as reacting with another monomer. Therefore, the initiation and propagation processes occur in parallel, and the polymer density and the average chain length continue to increase. In the MBE process, as the cluster size becomes larger, the clusters start contacting each other and form larger clusters. When this happens, the cluster density decreases. But throughout the whole process, the average cluster size keeps on increasing with time. In the VDP process, even when two polymers come into contact with each other, they usually do not react with each other. In this case those connected polymers form local rings, and a monomer deposited into one of these rings can neither react with existing long-chain polymers nor escape from the ring. Therefore, the chain initiations dominate the growth process, and the small chain polymer density increases dramatically while the long-chain polymer distribution remains unchanged. Thus the average chain length or weight decreases due to the formation of a large amount of short-chain polymers. However, in the limit $G\rightarrow0$, both the VDP model and MBE model become random deposition.

B. Rate equations of polymerization in the VDP growth model

Neglecting the direct capture of deposited monomers by polymers, the rate equation would have the following exact form ($\theta < \theta_p$) [9,11]:

$$\frac{dN_1}{dt} = F - k_1 N_1^2 - N_1 \sum_{L \geq 2} k_L N_L , \tag{7}$$

$$\frac{dN_L}{dt} = N_1 (k_{L-1} N_{L-1} - k_L N_L), \quad L > 1, \tag{8}$$

where k_L is the reaction rate of a monomer with a polymer of chain length $L(L=1,2,...)$. In our PVD model, $k_L \propto D$ is a constant. Since $F = 1/512^2$, the solution has the following scaling forms:

$$W \sim G^{1/3} \theta^{2/3}, \tag{9}$$

$$N \sim G^{1/3} \theta^{1/3}, \tag{10}$$

i.e., $\chi = \frac{1}{3}$ and $z = \frac{2}{3}$. These results are consistent with our Monte Carlo simulation result, $\chi = 0.302 \pm 0.002$ and $z = 0.69 \pm 0.02$. In contrast, in MBE processes, the rate constant k will closely depend on the cluster size [9]. Therefore, in a certain regime, MBE processes result in different scaling exponents as compared to those of the VDP process [9].

For higher coverages ($\theta > \theta_p$), because of the formation of the network structure, k_L is no longer constant. Rather, it is a variable depending on both the coverage and the surface spatial correlation [13,14]. Therefore the scaling breaks down. However, the explicit form for k_L in this case is unknown.

C. Comparison of the VDP growth model with DLSAW and Meakin's models

The relation between the DLSAW model and our VDP model is the same as the relation between the diffusion-limited aggregation (DLA) model and the MBE model. The DLSAW model will apply in the following cases: First, when the polymer chains are very long, from the above discussion, $W \propto G^{\chi}$, the growth is close to the DLSAW model. In fact, when $G \to \infty$, the VDP model becomes exactly the DLSAW model. Second, if the distance l between polymers is large compared to the polymer end-to-end distance R, DLSAW will occur. This requires small coverage θ since the average distance between polymers is $l \propto 1/\sqrt{N}$ where N is the polymer density. The average length of the polymer is $\overline{L} = \theta/N$. From Eq. (1), we obtain the ratio of the average polymer end-to-end distance R to the average distance l between polymers as

$$R/l = \left(\frac{\theta_1}{N} \right)^{\nu} N^{1/2}. \tag{11}$$

Substituting Eq. (4) into Eq. (11), we have

$$R/l \propto \theta^{\nu + (1-z)(\nu - 1/2)} G^{\chi(\nu - 1/2)}. \tag{12}$$

The crossover from DLSAW to non-DLSAW happens when $R/l \sim 1$, which imposes a crossover coverage θ_x,

$$\theta_x \propto G^{\chi(1/2-\nu)/[2\nu - z\nu + (z-1)/2]}, \tag{13}$$

so that DLSAW behavior will only be seen for $\theta < \theta_x$. Therefore, at low coverages, for which the monomer can walk randomly and freely, we obtained an exponent ν from our simulations which is close to the value obtained from the DLSAW model and the scaling for the polymer chain distribution. This agrees reasonably well with Fig. 14 for which DLSAW behavior is only seen for $\theta = 0.019$–0.191. Since $\nu \approx 0.774$, $\chi \approx \frac{1}{3}$, and $z \approx \frac{2}{3}$, the exponent in Eq. (13) is negative, which means θ_x decreases when G increases. This is consistent with our results observed in Figs. 6–8. Lastly, DLSAW will occur when the nucleation rate is small compared to the attachment rate. This will happen if the monomer density is less than the polymer density, which again requires small θ. However, as θ increases, the excluded volume principle confines the random walks. The monomer can only move in a small area, and keeps on interacting with long-chain polymers. This modifies the DLSAW process and eventually makes the polymer chain compact. Meakin's model extended DLSAW to describe the formation of multipolymer chains from a solution [7]. In his model, only one walker is active unless it terminates at the boundary of the lattice or reacts with an active site of the polymer. There is no competition between the deposition and diffusion. This model can approximately describe linear polymers grown from very dilute solutions, for which the diffusion limits all of the kinetic processes. The growing long-chain polymers can shadow short-chain polymers due to this diffusion-limited process. One longest chain will keep on growing and other short chains cease growth. Thus after a long time, this growth model becomes DLSAW. However, in our VDP model, there exist both deposition and diffusion processes. The competition of these two processes will give different dynamic behaviors. The chain configuration changes with the ratio G as well as with the deposition time. At low surface coverages, the chain distribution shows a certain chain length selection (peaks in the distribution), while at high coverages, small chains emerge rapidly with coverage due to the confinement caused by long-chain polymers. The longer-chain polymers remain intact.

In this simple VDP model, we did not consider the effects of interpolymer interactions or polymer relaxation. Those effects are similar to the effects of edge diffusion and step barrier in MBE growth, and one would expect that those effects tend to make the morphologies and chain configurations very different. For example, the attractive intermolecular force tends to make polymer chains more compact, while the repulsive intermolecular force extends the chains. We hope the present simulation work will stimulate more studies of VDP growth.

ACKNOWLEDGMENTS

This work is supported by the NSF. A. R. H. is supported by the NSF REU (Research Experience for Undergraduates). The authors thank Dr. Jacques G. Amar for his valuable comments.

[1] T.-M. Lu and J. A. Moore, Mater. Res. Bull. **20**, 28 (1997), and references therein; *Polymers for Electronic and Photonic Applications*, edited by C. P. Wong (Academic, Boston, 1993).
[2] W. F. Beach, C. Lee, D. R. Bassett, T. M. Austin, and O. Olson, in *Encyclopedia of Polymer Science and Engineering*, 2nd ed. (Wiley, New York, 1989), Vol. 17, p. 990.
[3] W. F. Beach, Macromolecules **11**, 72 (1977).
[4] S. Ganguli, H. Agrawal, B. Wang, J. F. McDonald, T.-M. Lu, G.-R. Yang, and W. N. Gill, J. Vac. Sci. Technol. **15**, 3138 (1997).
[5] P. G. de Gennes, *Scaling Concepts in Polymer Physics* (Cornell University Press, Ithaca, NY, 1979).
[6] R. M. Bradley and D. Kung, Phys. Rev. A **34**, 723 (1986).
[7] P. Meakin, Phys. Rev. A **37**, 2644 (1988).
[8] M. C. Bartelt and J. W. Evans, Phys. Rev. B **46**, 12 675 (1992).
[9] J. G. Amar, F. F. Family, and P.-M. Lam, Phys. Rev. B **50**, 8781 (1994).
[10] P. Jensen, A.-L. Barabási, H. Larralde, S. Havlin, and H. E. Stanley, Phys. Rev. B **50**, 15 316 (1994).
[11] G. S. Bales and D. C. Chrzan, Phys. Rev. B **50**, 6057 (1994).
[12] M. Schroeder, *Fractals, Chaos, and Power Laws* (Freeman, New York, 1991).
[13] J. G. Amar and F. Family, Surf. Sci. **382**, 170 (1997).
[14] S. Jiu, L. Bönig, and H. Metiu, Surf. Sci. **392**, L56 (1997).